POLITECNICO
MILANO 1863

ORBITAL MECHANICS ASSIGNMENT:
INTERPLANETARY AND PLANETARY EXPLORER MISSION

Professors: Camilla Colombo
Juan Luis Gonzalo Gomez
Francesca Scala
Giacomo Borelli

Group ID: 11

Marco Adorno
ID: 10565401
969305
Giuseppe Enricomaria Esposito
ID: 10804371
970081
Davide Gravina
ID: 10570605
964027
David Reina
ID: 10526269
953171

Academic year: 2020/2021

TABLE OF CONTENTS

1 SYMBOLS

a_{3body}	Acceleration perturbation due to Moon presence	$[km/s^2]$
$\overrightarrow{a_{J2}}$	Acceleration perturbation due to $J2$ perturbation	$[km/s^2]$
$\overrightarrow{a_{pert}}$	Total acceleration perturbation	$[km/s^2]$
a_{pert}^{RSW}	Perturbing acceleration in the RSW reference frame	$[km/s^2]$
δ_1	Radius of the neighbourhood of $t_{1,ga}$	$[days]$
δ_2	Radius of the neighbourhood of $t_{2,ga}$	$[days]$
δ_3	Radius of the neighbourhood of $t_{3,ga}$	$[days]$
Δt	Time of flight	$[days]$
$\Delta t_{H_{E-M}}$	Time of flight of an Hohmann transfer between Earth and Mars	$[days]$
$\Delta t_{H_{J-E}}$	Time of flight of an Hohmann transfer between Jupiter and Earth	$[days]$
Δt_{flyby}	Fly-by duration	$[h]$
Δv	Mission cost	$[km/s]$
Δv_{flyby}	Fly-by change of velocity	$[km/s]$
Δv_{ga}	Genetic algorithm minimum Δv	$[km/s]$
$\Delta\lambda$	Difference of longitude	$[deg]$
θ	True Anomaly	$[deg]$
θ_f	True anomaly of the final point	$[deg]$
θ_i	True anomaly of the initial point	$[deg]$
a	Semi-major axis	$[km]$
e	Eccentricity	$[-]$
$E.D.$	Earliest departure	$[days]$
h_p	Altitude of the fly-by hyperbola perigee	$[km]$
i	Inclination	$[deg]$
$J2$	Second Zonal Harmonic	$[-]$
$\vec{K}$	Vector of the Keplerian elements	$[km, deg]$
$\dot{M}$	Linear change rate of Mean anomaly	$[rad/s]$
m/k	Ratio between number of Earth revolutions (m) and satellite orbits (k)	$[-]$
r	Magnitude of position vector of spacecraft	$[km]$
$\vec{r}$	Position vector of spacecraft	$[km]$
$r_{Earth-3body}$	Distance between Earth and Moon	$[km]$
$r_{sc-3body}$	Distance between spacecraft and Moon	$[km]$
R_E	Medium radius of Earth	$[km]$
R_p	Radius of perigee	$[km]$
SOI	Sphere of influence	$[-]$
T	Period of spacecraft's orbit	$[s]$
$\tilde{T}$	Spacecraft nodal period	$[s]$

$\widetilde{T}_e$	Greenwich nodal period	$[s]$
$t_{1,ga}$	Genetic algorithm departure date	$[days]$
$t_{2,ga}$	Genetic algorithm fly-by date	$[days]$
$t_{3,ga}$	Genetic algorithm arrival date	$[days]$
$T_{syn_{J-E}}$	Synodic period between Jupiter and Earth	$[days]$
t_1	Time of departure	$[days]$
t_2	Time of fly-by	$[days]$
t_3	Time of arrival	$[days]$
t_{comp}	Optimization algorithm computational time	$[s]$
T_{Earth}	Period of Earth	$[days]$
T_{Jup}	Period of Jupiter	$[days]$
T_{Mer}	Period of Mercury	$[days]$
$\vec{v}$	Velocity of spacecraft	$[km/s]$
$\vec{V}^-$	Fly-by incoming heliocentric velocity	$[km/s]$
$\vec{V}^+$	Fly-by outgoing heliocentric velocity	$[km/s]$
v_∞	Fly-by excess velocity	$[km/s]$
v_p	Velocity at perigee of the fly-by hyperbola	$[km/s]$
x	Position x axis component	$[km]$
y	Position y axis component	$[km]$
z	Position z axis component	$[km]$
μ	Gravitational constant of attractor	$[km^3/s^2]$
μ_{3body}	Gravitational constant of the Moon	$[km^3/s^2]$
μ_E	Gravitational constant of the Earth	$[km^3/s^2]$
ω	Argument of the perigee	$[deg]$
$\dot{\omega}$	Linear change rate of Argument of the perigee	$[rad/s]$
ω_E	Angular velocity of the Earth	$[rad/s]$
Ω	Right Ascension of the Ascending Node	$[deg]$
$\dot{\Omega}$	Linear change rate of Right Ascension of Ascending Node	$[rad/s]$

2 INTERPLANETARY MISSION

2.1 INTRODUCTION

The PoliMi Space Agency is carrying out a feasibility study for a potential Interplanetary Explorer Mission visiting three planets in the Solar System: Jupiter, Earth and Mercury. The focus of the study is to analyse all the possible transfer options from Jupiter to Mercury, using a powered gravity assist around the Earth, and determining the optimal departure, fly-by and arrival dates to minimize the cost of the mission (Δv).

2.2 DESIGN PROCESS

2.2.1 Constraints

The mission undergoes the following constraints:

- The earliest departure date is set to: $\mathbf{01/06/2030}$
- The latest arrival date is set to: $\mathbf{01/06/2070}$
- The minimum altitude of perigee for the fly-by hyperbola must be set to: $\mathbf{200\ km}$

2.2.2 Assumptions

To carry out the assignment, the patched conic method has been used. Doing so, the following assumptions[1] have been made:

- The sphere of influence (SOI) of each planet in their planetocentric frame is supposed infinite;
- The sphere of influence (SOI) of each planet in the heliocentric frame is supposed negligible;
- Fly-by time is considered negligible, with supposed uniform gravitational field around the planet;
- The initial heliocentric orbit is equal to the one of the departure planet;
- The final heliocentric orbit is equal to the one of the arrival planet;
- All manoeuvres are assumed to be instantaneous;
- Possible encounters with other planets and Solar Radiation Perturbation are ignored.

2.2.3 Preliminary estimations

As a preliminary reduction of the departure window, a study on the relative synodic period of the planets has been conducted (**TABLE 1**):

Synodic period of Jupiter w.r.t. Earth	$398.8699\ days$
Synodic period of Earth w.r.t. Mercury	$115.8774\ days$
Synodic period of Jupiter w.r.t. Mercury	$89.7916\ days$

Table 1: Relative synodic periods between the three planets.

The results show that if the largest synodic period ($T_{syn_{J-E}}$) is taken as an upper limit of the departure window, a consistent portion of the possible transfers is cut out. This happens because the synodic period is significantly shorter than the total transfer window set by the constraints. Therefore, the departure window has been limited to a single orbital period of Jupiter.

To limit the time window for the first transfer, from Jupiter to Earth, the time of flight of an Hohmann transfer between said two planets has been calculated and summed to the departure window limits. This technique has been chosen to cut out a category of transfers that surely was not convenient to perform. Particularly, the Hohmann transfer has been selected because the orbits of the planets are close to be coplanar and circular. Therefore, the Hohmann transfer would represent the optimum choice in this kind of situation[1]; this hypothesis allows to exclude all the transfers with a higher cost. The same has been done for the second transfer between Earth and Mercury. At last, it was checked that the latest time to perform the second transfer was less than the time window limit provided by the constraints.

The three time windows are displayed in **TABLE 2:**

Departure date window	
$E.D.$	$E.D. + T_{Jup}$
$01/06/2030$	$13/04/2042$
Flyby date window	
$E.D. + 70\%\ \Delta t_{H_{J-E}}$	$E.D. + T_{Jup} + 130\%\ \Delta t_{H_{J-E}}$
$29/04/2032$	$31/01/2045$
Arrival date window	
$E.D. + 70\%\ \Delta t_{H_{J-E}} + 70\%\ \Delta t_{H_{E-M}}$	$E.D. + T_{Jup} + 130\%\ \Delta t_{H_{J-E}} + 130\%\ \Delta t_{H_{E-M}}$
$12/07/2032$	$17/03/2046$

Table 2: Time windows selected for the phases of the transfer.

2.3 SOLUTION METHODS

The Δv optimization problem presents three degrees of freedom: the departure date from Jupiter, the fly-by date around Earth and the arrival date to Mercury. The aim of the process is to obtain the combination of these dates that returns the minimum Δv possible to perform the transfer. The procedure used consists in an initial implementation of a genetic algorithm, which finds the optimal solution to the Lambert problems and the powered gravity assist involved in the transfer, followed by a refinement using other two optimization methods: a gradient-based optimization and a grid search method. Afterwards, the best result was chosen as the final solution.

2.3.1 First optimization: genetic algorithm

The genetic algorithm was applied to the optimization problem using the MATLAB function `ga.m`. The algorithm searches for the minimum of a given function subjected to lower and upper boundary conditions. In the case of this study, the function used was the one of the complete interplanetary transfer, while the boundary conditions were given by the time windows shown in

TABLE 3. The solutions obtained were the departure ($t_{1,\mathrm{ga}}$), fly-by ($t_{2,\mathrm{ga}}$) and arrival ($t_{3,\mathrm{ga}}$) dates for an optimal Δv cost. This quantity was called Δv_{ga}.

DOF	Lower boundary	Upper boundary
Departure date	01/06/2030	13/04/2042
Fly-by date	29/04/2032	31/01/2045
Arrival date	12/07/2032	17/03/2046

Table 3: Boundary conditions for the genetic algorithm.

Since the procedures inside the algorithm have a random nature, the algorithm was run for five iterations and the best result was chosen.
The two fundamental parameters for convergence are the population size and the maximum number of generations. The population size must be large enough to generate a wide variety of permutations while the number of generations must be high enough to reach the convergence of the current run. Larger values for both parameters increase the probability that the global minimum is found, at the expense of computational time. A good compromise between the computational time and the quality of the convergence was found with a population size of 1000 and a maximum number of generations of 100.

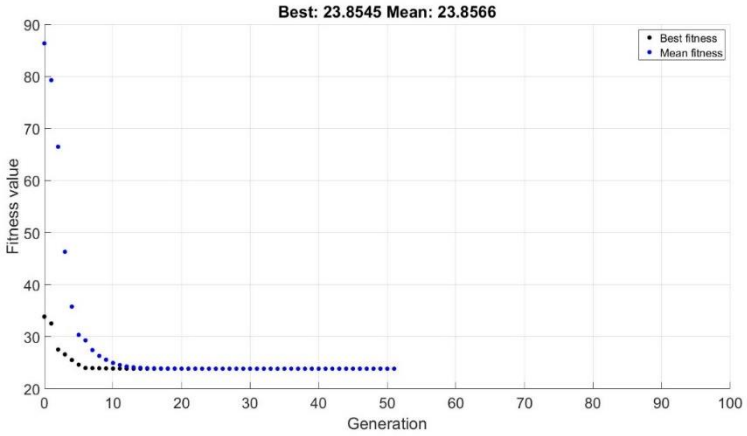

Figure 1: Convergence of the genetic algorithm

2.3.2 Second optimization

For the second part of the optimization, the results of the genetic algorithm ($t_{1,\mathrm{ga}}$, $t_{2,\mathrm{ga}}$, $t_{3,\mathrm{ga}}$), have been further refined with other two methods. The boundary conditions have been chosen in order to create a neighbourhood of the optimum solution in which the methods could perform the refinement. The neighbourhood has been generated adding and subtracting the terms δ_i, which can be taken arbitrarily. In the case of this study, the delta values are:

$$\delta_1 = \frac{T_{Earth}}{2} \qquad \delta_2 = T_{Earth} \cdot \frac{\delta_1}{T_{Jup}} \qquad \delta_2 = T_{Mer} \cdot \frac{\delta_1}{T_{Jup}}$$

Hence, the resulting boundaries for the method are shown in **TABLE 4**.

DOF	Lower boundary	Upper boundary
Departure time	$t_{1,\mathrm{ga}} - \delta_1$	$t_{1,\mathrm{ga}} + \delta_1$
Fly-by time	$t_{2,\mathrm{ga}} - \delta_2$	$t_{2,\mathrm{ga}} + \delta_2$
Arrival time	$t_{3,\mathrm{ga}} - \delta_3$	$t_{3,\mathrm{ga}} + \delta_3$

Table 4: Boundary conditions for the second optimization process

2.3.2.1 Gradient-based optimizer

A gradient-based optimizer was applied to the optimization problem using the MATLAB function `fmincon.m`. The algorithm searches for the minimum of a non-linear constrained multivariable function. The constraints applied can be of various nature, both linear and non-linear, but, as done for the genetic algorithm, linear constraints provided by the time windows have been used.
The initial guess of the minimum value, required by the command, was set as the value obtained from the genetic algorithm. This method was the most efficient in terms of computational time, with a waiting time of less than half a second.

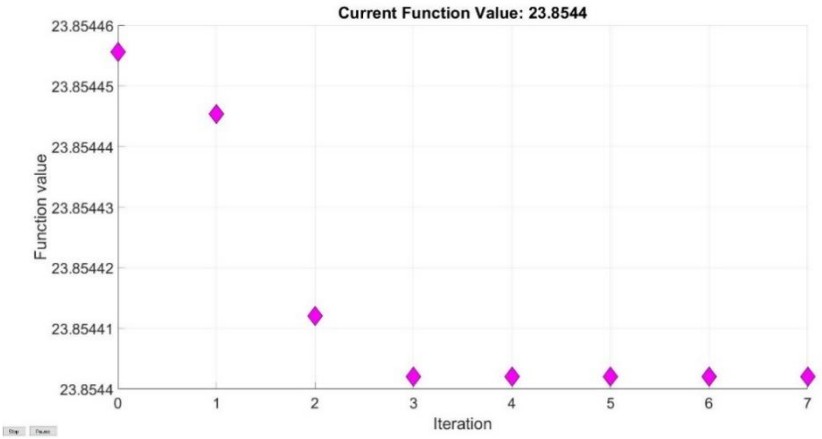

Figure 2: Convergence of the gradient-based algorithm

2.3.2.2 Grid search

The other alternative for a finer optimization was the grid search method. The grid is defined by an array of values set using as reference the value obtained from the genetic algorithm. The grid search consists in three nested loops that analyse all the possible combinations of departure dates, fly-by dates and arrival dates in the neighbourhood of the optimum found by the genetic algorithm. The optimum Δv is calculated using the following pseudo-code:

```
for all possible departure dates around t_1,ga
    for all possible fly-by dates around t_2,ga
        for all possible arrival dates around t_3,ga
            calculation of the total Δv of the transfer
        end
    end
end
```

The algorithm converges to the global minimum as the discretization of the grid is increased, but finer discretization causes a significant increase of computational time. In the case of this study the computational time was around 7 minutes.

2.4 RESULTS

TABLE 5 shows the results obtained with the three methods. As it can be noticed, the algorithms used for the second part of the optimization provided a slightly better result for the cost of the mission with respect to the genetic algorithm. The best result, both in terms of Δv and Δt, was obtained with the grid search algorithm, at the expense of computational time. The `fmincon.m` algorithm stopped its iterations near the initial value because it was already near a local minimum.

Method	t_1 $[mjd2000]$	t_2 $[mjd2000]$	t_3 $[mjd2000]$	Δt $[days]$	Δv $[km/s]$	t_{comp} $[s]$
G.A.	11705.8494	12903.3103	13949.6986	2243.8492	23.8545	104.4524
fmincon	11705.8483	12903.3100	13949.6979	2243.8496	23.8544	0.4215
Grid search	11881.0989	12915.5913	13952.7313	2071.6323	23.6279	396.3988

Table 5: Optimization algorithms results

The chosen dates to perform the transfer are reported in **TABLE 6**:

Departure date	$12/07/2032 - 14:22:30$
Fly-by date	$13/05/2035 - 02:11:27$
Arrival date	$15/03/2038 - 05:33:01$

Table 6: Chosen dates for the three phases of the transfer

The detailed report of the Δv cost for each manoeuvre is shown in **TABLE 7**:

Manoeuvre	Δv $[km/s]$
Injection in the first transfer leg	8.8694
Powered gravity assist	0.0063
Injection in the final orbit	14.7523
Total transfer	$\mathbf{23.6279}$

Table 7: Cost of each manoeuvre

2.5 FINAL TRAJECTORY CHARACTERIZATION

The Keplerian elements of the chosen trajectory legs are shown in **TABLE 8**, while the chosen strategy is displayed in **FIGURE 3**.

	a $[km]$	e $[-]$	i $[deg]$	Ω $[deg]$	ω $[deg]$	ϑ_i $[deg]$	ϑ_f $[deg]$
First transfer leg	$4.1868 \cdot 10^8$	0.8680	0.3935	52.1902	68.5723	175.8502	111.4277
Second transfer leg	$3.0779 \cdot 10^8$	0.8433	7.0936	52.1902	60.7631	119.2369	15.6349

Table 8: Keplerian parameters of the Lambert arcs

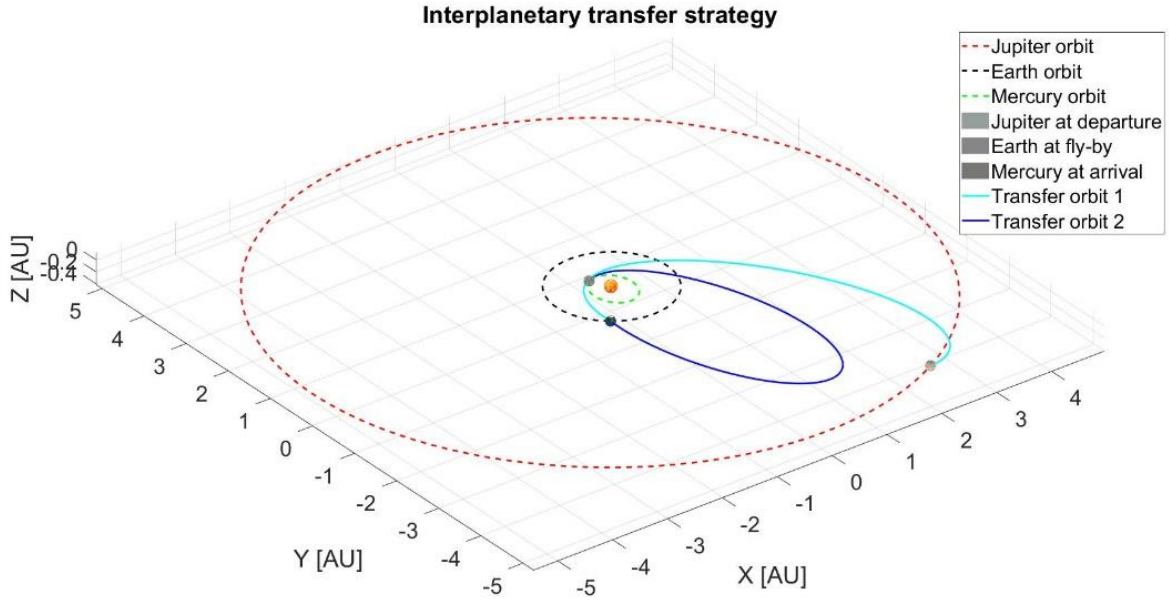

Figure 3: Trajectory of the total transfer

The fly-by incoming and outgoing heliocentric velocities of the spacecraft are:

$$\vec{V}^- = \begin{Bmatrix} 1.5826 \\ -37.9043 \\ -0.1682 \end{Bmatrix} [km/s] \quad \vec{V}^+ = \begin{Bmatrix} 0.3833 \\ -36.2912 \\ -2.8063 \end{Bmatrix} [km/s] \quad \Delta v_{flyby} = \left\| \vec{V}^+ - \vec{V}^- \right\| = 3.3166\ km/s$$

The incoming and outgoing hyperbolic trajectories are characterized by the parameters reported in **TABLE 9**.

	$h_p\ [km]$	$v_p\ [km/s]$	$v_\infty\ [km/s]$	$e\ [-]$	$a\ [km]$
Incoming hyperbola	1127.0321	30.7293	29.0206	17.4983	−473.2876
Outgoing hyperbola	1127.0321	30.7356	29.0272	17.5059	−473.0710

Table 9: Parameters of incoming and outgoing hyperbolic trajectories

The total duration of the fly-by, considering a finite SOI is:

$$\Delta t_{flyby} = 17{,}8397\ hours$$

The hyperbolic trajectories are represented in **FIGURE 4**:

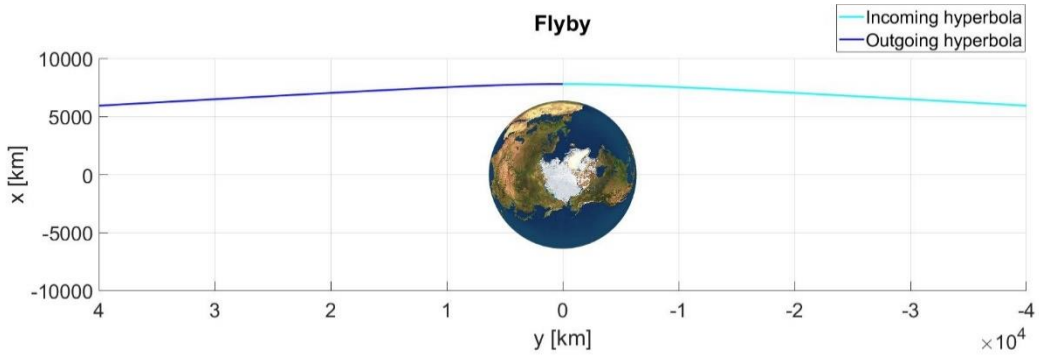

Figure 4: Fly-by hyperbolic trajectory

2.6 DISCUSSION

From the tables of the costs of the manoeuvres, it can be seen that the last transfer, going from Earth to Mercury, is the most expensive due to the change of plane to get on Mercury's orbit.

The fly-by cost is the lowest of the entire transfer because the turn angle of the two hyperbolas is almost identical. This means that the two different hyperbolic trajectories can be considered as a single one and therefore the cost of the manoeuvre at the perigee is irrisory compared to the others.

As it can be seen from the porkchop plots in **FIGURES 5-6**, the minimum of the single transfer arc is different from the one chosen to perform the mission. However, it has to be kept in mind that the minimum of each Lambert arc doesn't necessarily correspond to the global minimum of the complete transfer, as confirmed by the graphs below:

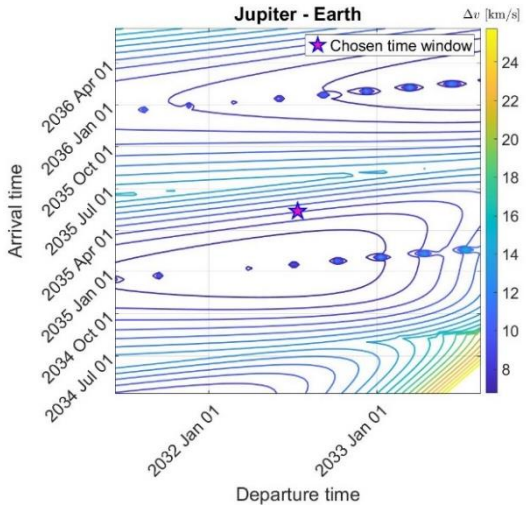

Figure 5: Porkchop plot of the Lambert arc from Jupiter to Earth

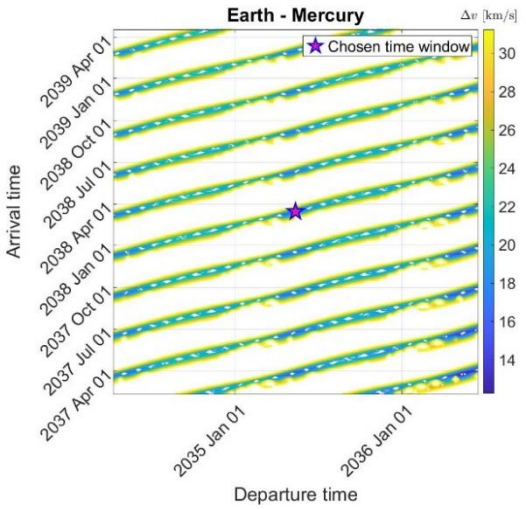

Figure 6: Porkchop plot of the Lambert arc from Earth to Mercury

To further decrease the total cost of the mission, multiple fly-bys could be exploited. In the case of this study, a fly-by around Mars or around Venus could have been performed. Regarding the latter option, a real application can be seen in the mission "BepiColombo"[4], whose objective is to reach the orbit of Mercury, as done in this study, although starting from Earth.

3 PLANETARY EXPLORER MISSION

3.1 INTRODUCTION

The PoliMi Space Agency plans to launch an Earth observation satellite. This study examines the proposed orbit and the ground track of the spacecraft, the effects of the presence of the Moon and the $J2$ perturbation. A repeating ground track is desired and a method to achieve it is therefore presented. Two different numerical orbital propagation methods are used, and the results are compared and discussed.

3.2 MISSION DATA

The orbit was characterized by the parameters displayed in **TABLE 10**:

$\boldsymbol{a}$	$3.9899 \cdot 10^4\ km$
$\boldsymbol{e}$	0.2510
$\boldsymbol{i}$	56.6144°
$\boldsymbol{\Omega}$	0.00°
$\boldsymbol{\omega}$	0.00°
$\boldsymbol{\theta}$	0.00°
$\boldsymbol{R_p}$	$29884.351\ km$
$\boldsymbol{m}$	1
$\boldsymbol{k}$	1
$\boldsymbol{T}$	$0.9180\ days$

Table 10: Assignment data

The spacecraft travels in a high altitude Earth orbit and completes one orbit almost every one revolution of the Earth.

3.3 PERTURBATION MODELLING

3.3.1 J2 effect

Earth oblateness and spheroid structure results in a non-uniform gravitational field. The zonal effect of the real gravitational field can be modelled using a series of spherical harmonics, in which the dominating term is $J2$ (two orders of magnitude higher than the following term). The acceleration caused by this non-homogeneity on the spacecraft's orbit can be represented by the following equation[1]:

$$\overrightarrow{a_{J2}} = \frac{3}{2} \cdot \frac{J2 \cdot \mu_E \cdot R_E}{r^4} \cdot \left[\frac{x}{r} \cdot \left(5 \cdot \frac{z^2}{r^2} - 1 \right) \vec{\imath} + \frac{y}{r} \cdot \left(5 \cdot \frac{z^2}{r^2} - 1 \right) \vec{\jmath} + \frac{z}{r} \cdot \left(5 \cdot \frac{z^2}{r^2} - 3 \right) \vec{k} \right]$$

The principal effects of this perturbation are nodal regression and perigee precession.

3.3.2 Moon presence effect

Being in a high altitude Earth orbit, one of the most prevalent perturbations is the direct gravitational attraction of the Moon. This happens because the distances between the spacecraft and Earth and the spacecraft and the Moon, at such high altitudes, become comparable:

$$a_{3body} = \mu_{3body} \cdot \left(\frac{r_{sc-3body}}{r_{sc-3body}^3} - \frac{r_{Earth-3body}}{r_{Earth-3body}^3} \right)$$

As we can see from the equation[1], the first term in the parenthesis becomes comparable with the second one. The principal effects of this perturbation are secular changes in e, i and ω.

3.4 INTEGRATION METHODS

The two-body problem with non-conservative perturbations can be solved by numerical integration in Cartesian coordinates of the equation of motion of the perturbed two-body problem, or by numerical integration of the Gauss Planetary Equations (GPE), which give the evolution in time of the Keplerian elements of the orbit. Both integration methods were implemented using the MATLAB solver `ode113` with relative tolerance equal to 10^{-13} and absolute tolerance equal to 10^{-14}.

3.4.1 Integration of the equation of motion

The first method involved the numerical integration of the equation of motion of the perturbed two-body problem, written in a state-space form as follows[1]:

$$\frac{d}{dt}\begin{Bmatrix} \vec{r} \\ \vec{v} \end{Bmatrix} = \begin{Bmatrix} \vec{v} \\ -\frac{\mu}{r^3}\vec{r} + \overrightarrow{a_{pert}} \end{Bmatrix}$$

3.4.2 Integration of Gauss planetary equations

Gauss Planetary Equations provided an expression for the time derivative of each Keplerian element of the orbit. Integrating these equations for each time-step returned the complete time history of the Keplerian elements along the desired time period. The equations were integrated in this form:

$$\frac{d}{dt}\{\vec{K}\} = fun\left(\overrightarrow{K}, a_{pert}^{RSW}\right)$$

3.5 GROUND TRACKS

The Satellite ground track was evaluated in three different timesteps (1 orbit, 1 day, 10 days) in the unperturbed case and in perturbed case considering only the $J2$ effect.

In the unperturbed case, the only effect shown is the eastward rotation of Earth, evaluated with the formula[1]: $\Delta\lambda = T \cdot \omega_E = 331.36°$. This phenomenon should affect the ground track with a westward shift, although in the figures is shown as an eastward shift due to the high value of $\Delta\lambda$.

Regarding the ground track repetition, for the unperturbed motion the only effect to consider is again the rotation of the Earth. The semi-major axis required for the ground track repetition is obtained imposing the following relation[1] between the spacecraft and the Earth orbital period:

$$\frac{T}{T_E} = \frac{m}{k}$$

where k and m are the number of revolutions of the spacecraft and the Earth respectively after which the repetition must take place. Given the m and k values of this case study, the repeating ground track semi-major axis was calculated:

$$a_{rep} = 42166.17\ km$$

In the perturbed case, in addition to the effect caused by the rotation of the Earth, it must be considered the secular evolution of the Keplerian elements caused by the $J2$ perturbation, which modifies the values of the orbital period. The repetition of the ground track could still be obtained introducing the more general satellite and Greenwich nodal periods ($\tilde{T}, \tilde{T}_E$), affected by the secular variation of Ω, ω, and M. The final equation is[1]:

$$\frac{m}{k} = \frac{\tilde{T}}{\tilde{T}_E} = \frac{\omega_E - \dot{\Omega}}{n + \dot{\omega} + \dot{M}}$$

where n is the mean angular motion of the satellite. The secular variations of the Keplerian elements due to $J2$ perturbation are expressed in the following way[1]:

$$\dot{\Omega} = -\frac{3}{2} \cdot \frac{\sqrt{\mu} \cdot J2 \cdot R_E^2}{a^{7/2} \cdot (1 - e^2)^2} \cdot \cos(i)$$

$$\dot{\omega} = -\frac{3}{2} \cdot \frac{\sqrt{\mu} \cdot J2 \cdot R_E^2}{a^{7/2} \cdot (1 - e^2)^2} \cdot \left(\frac{5}{2} \cdot \sin^2(i) - 2\right)$$

$$\dot{M} = -\frac{3}{2} \cdot \frac{\sqrt{\mu} \cdot J2 \cdot R_E^2}{a^{7/2} \cdot (1 - e^2)^2} \cdot \left(1 - \frac{3}{2} \cdot \sin^2(i)\right)$$

In particular, the secular effects for the assigned orbit cause a westward drift of the line of nodes and an advance of the perigee in the direction of the satellite motion. Solving the implicit equation for the semi-major axis[1], the following value was obtained:

$$a_{rep_{J2}} = 42165.77\ km$$

In the following figures, the required ground tracks are reported:

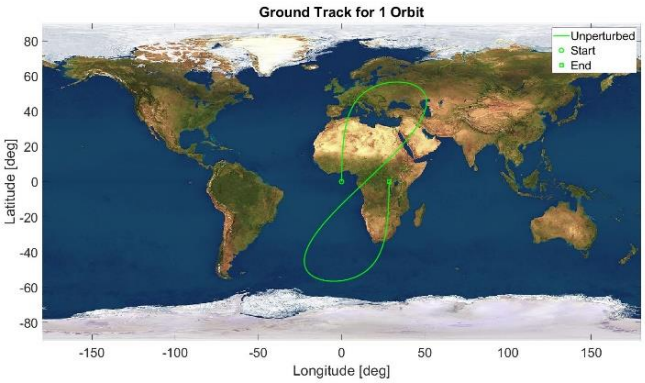

Figure 7: Unperturbed ground track for 1 orbit

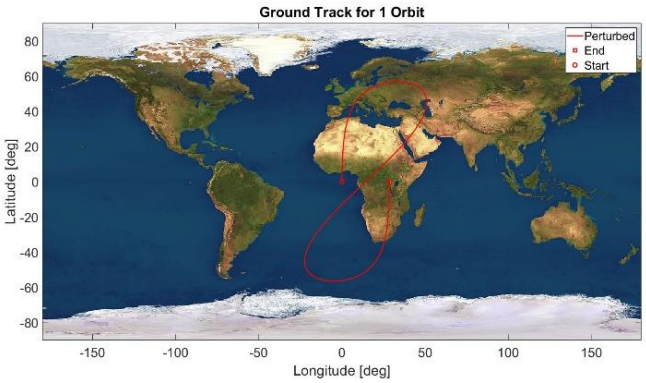

Figure 8: Perturbed ground track for 1 orbit

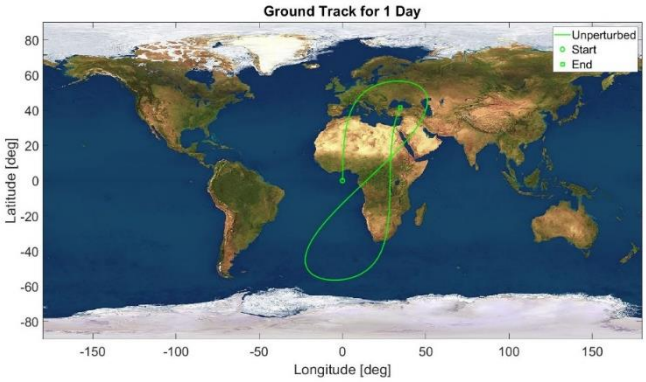

Figure 9: Unperturbed ground track for 1 day

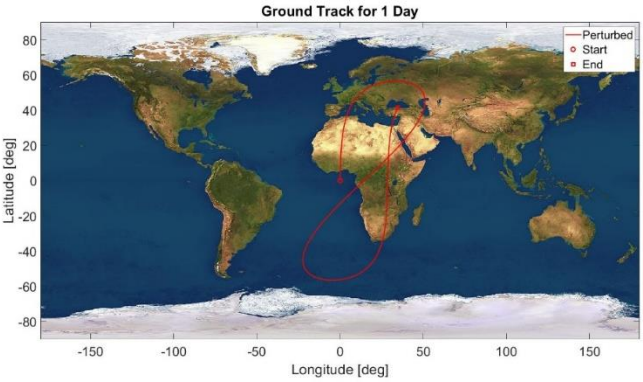

Figure 10: Perturbed ground track for 1 day

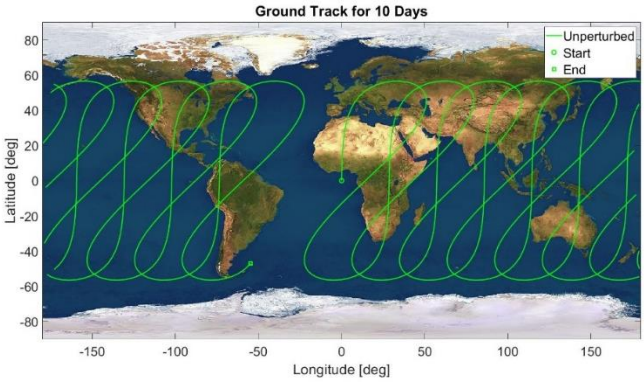

Figure 11: Unperturbed ground track for 10 days

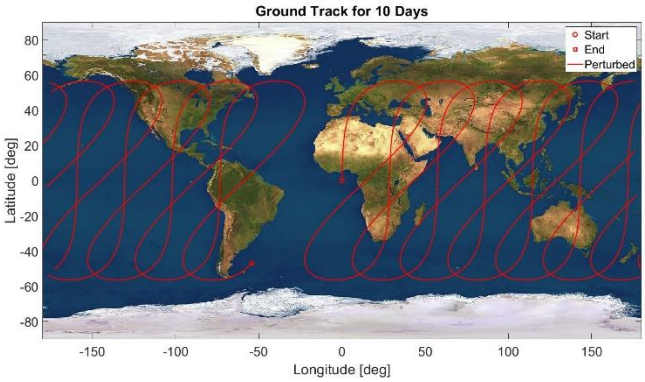

Figure 12: Perturbed ground track for 10 days

In the following figures, the required repeating ground tracks are reported:

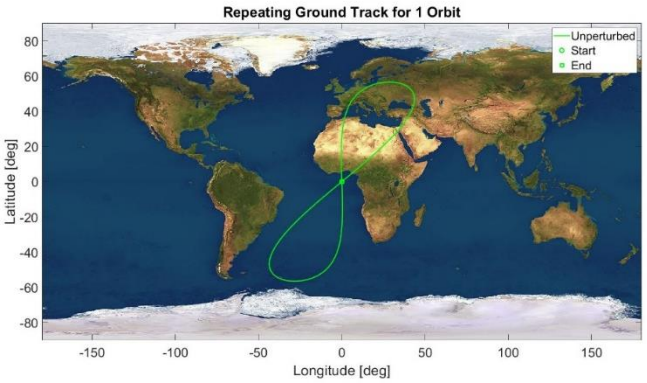

Figure 13: Unperturbed repeating ground track for 1 orbit

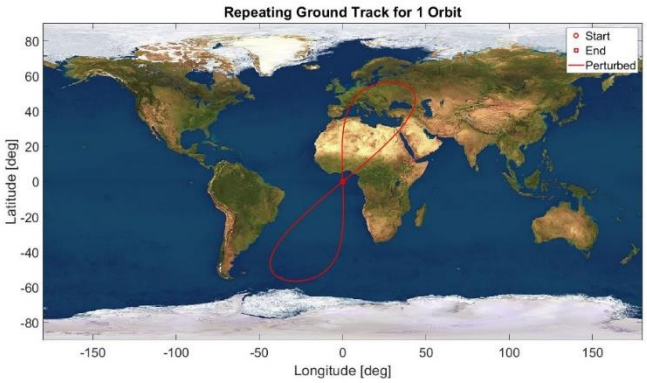

Figure 14: Perturbed repeating ground track for 1 orbit

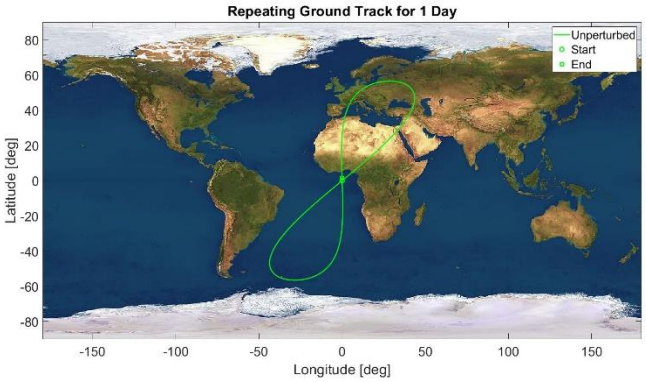

Figure 15: Unperturbed repeating ground track for 1 day

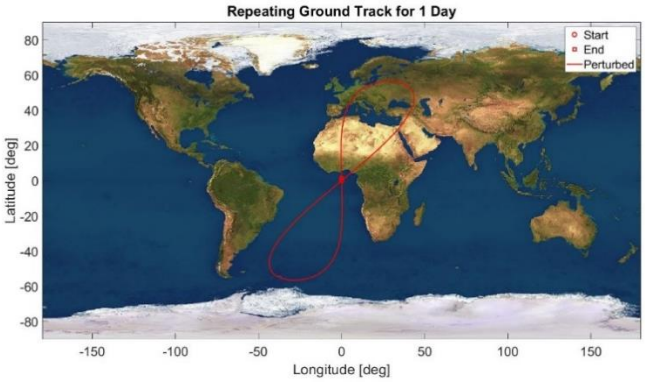

Figure 16: Perturbed repeating ground track for 1 day

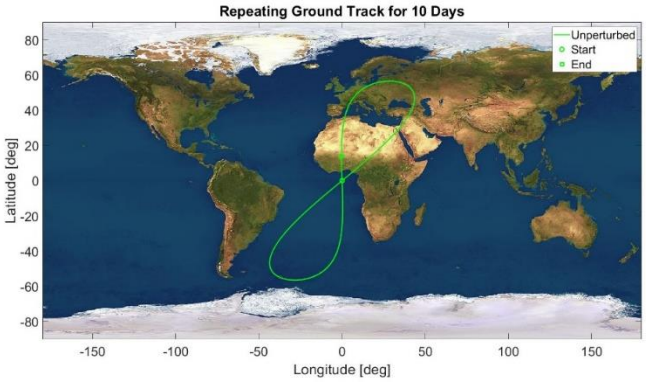

Figure 17: Unperturbed repeating ground track for 10 days

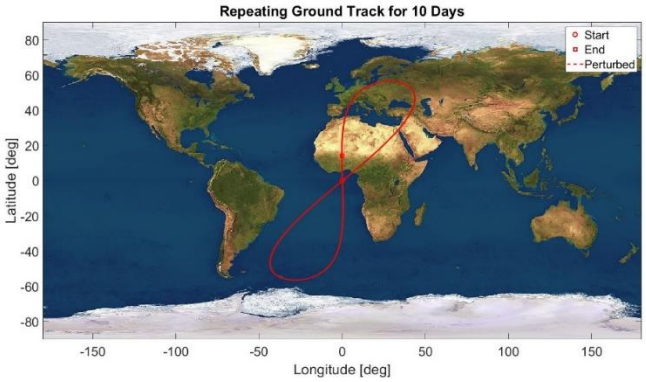

Figure 18: Perturbed repeating ground track for 10 days

From the graphs it can be noticed that, at least in the short period, the difference between the perturbed and unperturbed ground track, both for the repeating and non-repeating case, is almost negligible, because the $J2$ effect is much smaller than the one provoked by the rotation of the Earth. Physically, this happens because the large semi-major axis of the orbit considered significantly decreases the effect of $J2$, as can be seen from the equations[1]. In addition, the ground track repeats almost perfectly in both cases, and the small differences that are present can be justified by numerical errors in the propagation and approximated model assumptions.

3.6 ORBIT PROPAGATION

In the following figures, the evolution of the Keplerian elements of the orbit is shown, comparing the integration of the equation of motion and the integration of the Gauss Planetary Equations through the relative error between the two results.

The following behaviours can be distinguished:

- Secular effects on Ω and ω due to the $J2$ perturbation;
- Secular effects on e, i, ω due to the Moon perturbation;
- Short and long periodic oscillations on all the elements due to the combination of the two perturbing effects.

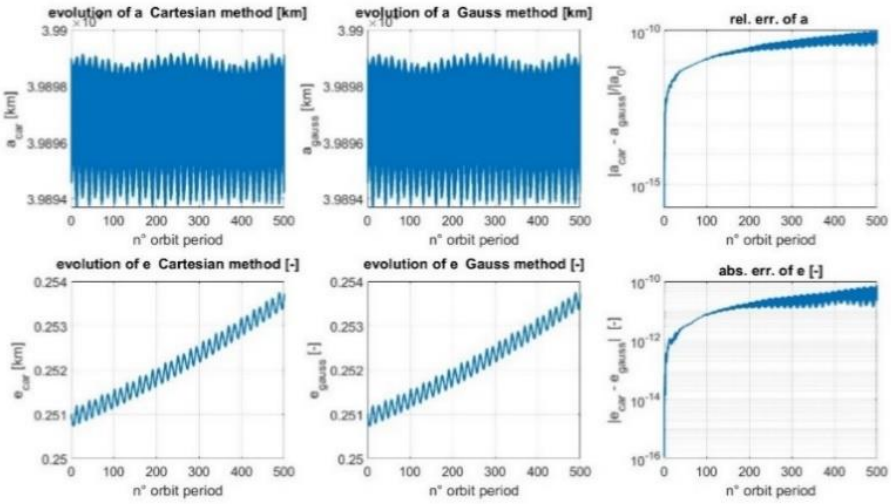

Figure 19: Evolution of the semi-major axis and eccentricity and relative and absolute errors between the two methods

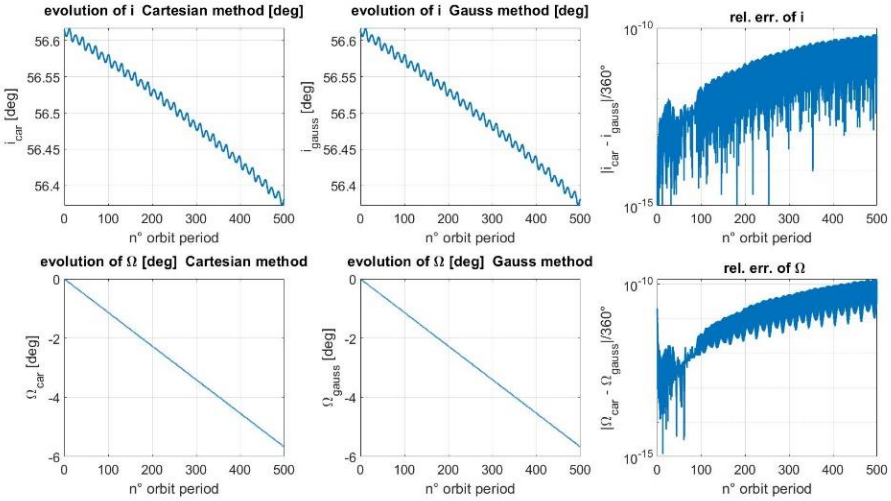

Figure 20: Evolution of inclination and Ω, and relative errors between the two methods

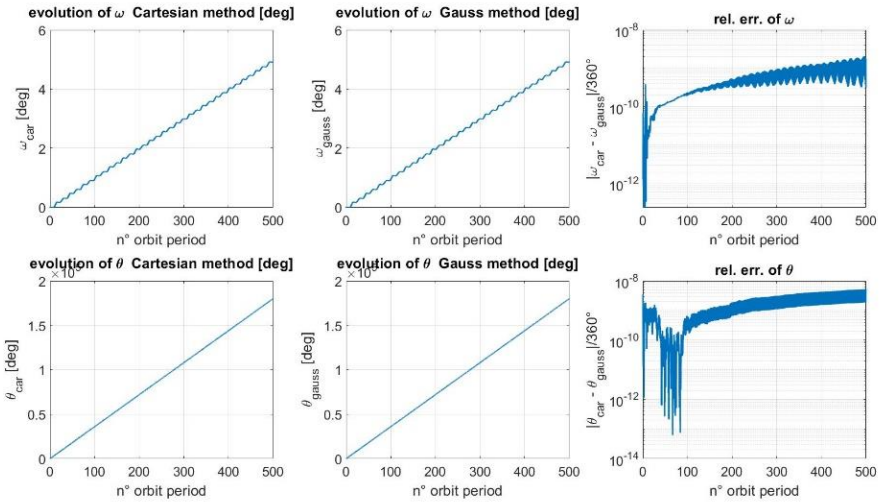

Figure 21: Evolution of ω and θ and relative errors between the two methods

The graphs highlight an almost equal behaviour in terms of accuracy for the two propagation methods, whereas the simulations showed a slightly higher computational efficiency for the Gauss method, which was almost 1 second faster in the case of the 10000 points used for the time discretization. This difference in computational time increased with a finer discretization of the time interval. In addition, the Cartesian propagation requires a conversion of the orbital state into Keplerian elements at each iteration, making it even more time consuming and numerically cumbersome. Because of these considerations, further computations for orbit propagation were carried out using the Gauss method.

In **TABLE 11** are reported the maximum errors between the two computations:

KEPLERIAN ELEMENT	RELATIVE ERROR
a	$1.1232 \cdot 10^{-10}$
e	$7.5762 \cdot 10^{-11}$
i	$1.1669 \cdot 10^{-12}$
Ω	$2.4606 \cdot 10^{-12}$
ω	$3.5793 \cdot 10^{-11}$
ϑ	$9.2677 \cdot 10^{-11}$

Table 11: Maximum errors between the results of the two computations (Cartesian, GPE).

3.7 REPRESENTATION OF THE ORBIT EVOLUTION

The orbit evolution considering the previous perturbations was computed during a period of 25 years, or 10000 orbits.

The complete evolution of the orbit is shown in **FIGURE 22**.

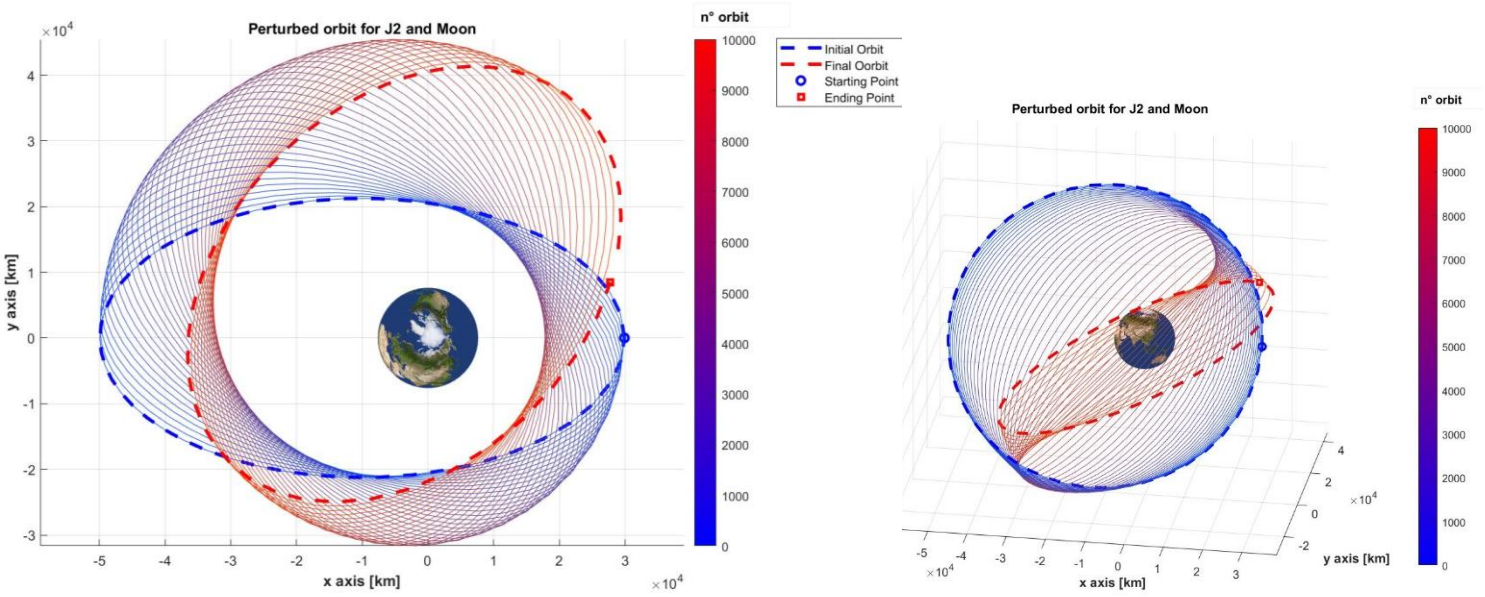

Figure 22: Figure on the left shows the POV of complete orbit, from above. Figure on right shows the same plot, with another POV, to show the 3D shift of orbit, during the period considered.

In **TABLE 12** are reported the values of the Keplerian elements for the initial orbit and for the final orbit of the propagation.

INITIAL ORBIT PARAMETERS:					
$\boldsymbol{a}$	$\boldsymbol{e}$	$\boldsymbol{i}$	$\boldsymbol{\Omega}$	$\boldsymbol{\omega}$	$\boldsymbol{\vartheta}$
$39899.0\ km$	0.2510	$56.6144°$	$0.0°$	$0.0°$	$0.0°$
FINAL ORBIT PARAMETERS:					
$\boldsymbol{a}$	$\boldsymbol{e}$	$\boldsymbol{i}$	$\boldsymbol{\Omega}$	$\boldsymbol{\omega}$	$\boldsymbol{\vartheta}$
$39897.54\ km$	0.3200	$46.6746°$	$-136.52°$	$76.14°$	$0.0°$

Table 12 : Keplerian elements of initial and final orbit of 10000 orbit propagation.

3.8 FILTERING OF KEPLERIAN ELEMENTS

Two different oscillatory behaviours can be noticed among all the Keplerian elements: short periodic oscillations (with a period of ~ 1 orbital period) and long periodic oscillations (with a period of ~ 15 orbital periods). In order to recover only the long periodic and secular effects, a low-pass filter has been applied to the propagated elements. In particular, the filter was implemented through the MATLAB function `movmean.m`, which computes at each point of the array the mean value (moving mean) of a time window centred at that point. The length of the time window, which is defined a priori by the user and is related to the cut-off frequency of the filter, was set equal to the two

oscillatory periods (1 and 15 orbital periods), to recover the long periodic and secular behaviours, or just the secular behaviour, respectively. The results are shown in **FIGURE 23** (the initial and final plot's behaviour of secular effect is not considered, due to a computational error caused at the starts and ends of the dataset):

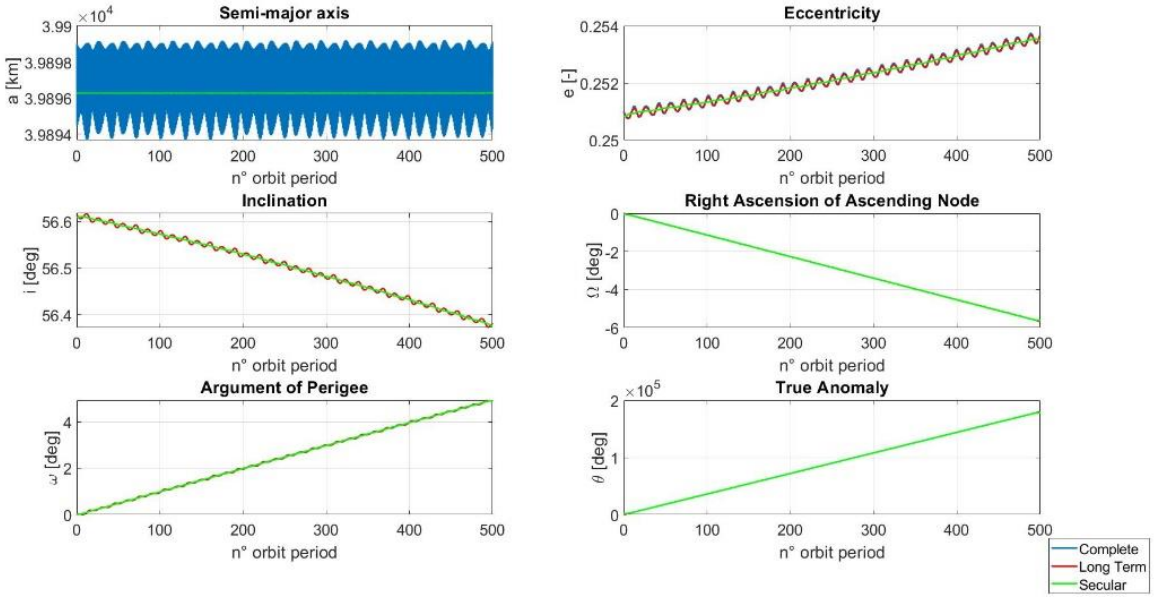

Figure 23: Filtering of Keplerian elements

3.9 REAL DATA COMPARISON

In order to validate the numerical propagation, it was performed a comparison using the data of an accurate model made by NASA HORIZONS system[2]. The satellite chosen as reference was the ZHONGXING-7[3], a Chinese spacecraft for telecommunications launched in August of 1996 and now set on a graveyard orbit at almost the same altitude of the assigned orbit. Being on a graveyard orbit, the spacecraft resents only of the acting perturbations and does not undergo any kind of manual orbital correction. Orbital manoeuvres would have prevented the accurate comparison between the implemented model for the perturbations and a real case since the modifications of the orbit would have been corrected.

TABLE 13 shows the numerical results of maximum errors between real data and the considered Gauss propagation:

KEPLERIAN ELEMENT	RELATIVE ERROR
a	$1.0448 \cdot 10^{-4}$
e	0.0027
i	$7.3473 \cdot 10^{-4}$
Ω	0.0018
ω	0.0037
ϑ	$6.6029 \cdot 10^{-4}$

Table 13: Maximum relative errors between two sets of data (Real and Gauss propagation).

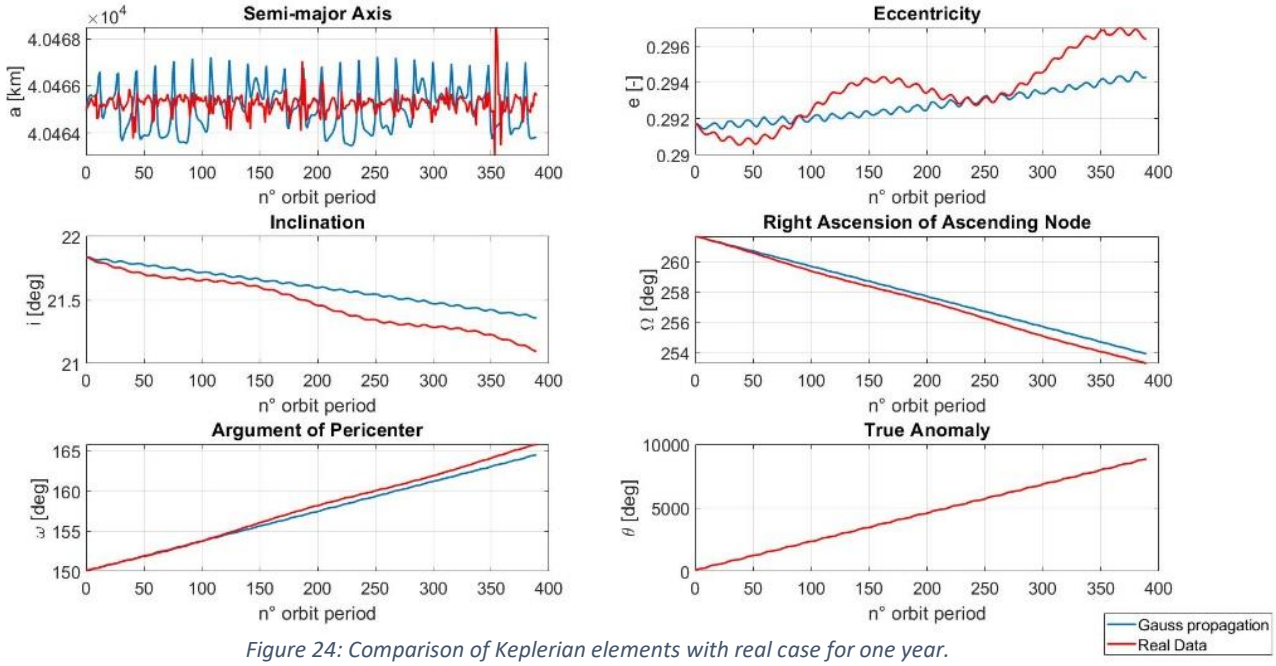

Figure 24: Comparison of Keplerian elements with real case for one year.

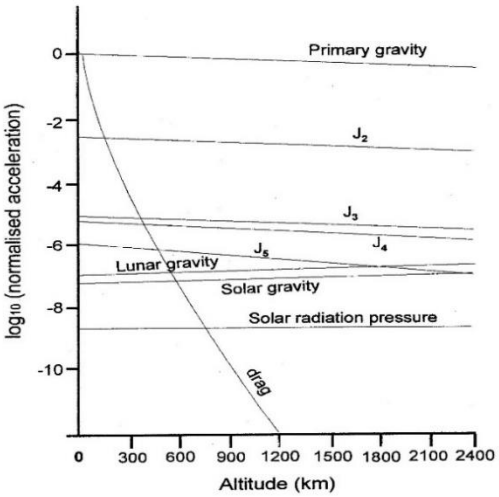

Figure 25: Representations of orders of magnitude of the principal perturbation effects[1]

As it can be seen from the table and the graphs in **FIGURE 24**, the evolution of the Keplerian elements between the two orbits give a very good approximation for almost all terms and become slightly different during the propagation. The main differences are especially for some terms like (e , i , Ω , ω) that describe an additional oscillatory behaviour, in the long term, and a higher secular effect.

This particular behaviour could be mainly caused by the Solar Radiation Pressure effect, which was not modelled in the case of this study, but is particularly relevant in this real application, especially because this satellite is in a high altitude Earth orbit[1].

4 REFERENCES

[1] Curtis, H.D., *Orbital Mechanics for Engineering Students*, 2005, Elsevier Butterworth-Heinemann, MA, USA.

[2] NASA/JPL's HORIZONS (https://ssd.jpl.nasa.gov/horizons.cgi)

[3] LCH team SPACE-TRACK (https://www.space-track.org/)

[4] ESA's BepiColombo fact sheet (https://sci.esa.int/web/bepicolombo/-/47346-fact-sheet)